Received: 11 October 2022 | Revised: 4 February 2023 | Accepted: 19 March 2023

DOI: 10.1002/aic.18099

AIChE JOURNAL

RESEARCH ARTICLE

Transport Phenomena and Fluid Mechanics

New understanding from intestinal absorption model: How physiological features influence mass transfer and absorption

Yifan Qin[1,2] | Xiao Dong Chen[1] | Aibing Yu[2,3] | Jie Xiao[1]

[1]School of Chemical and Environmental Engineering, College of Chemistry, Chemical Engineering and Materials Science, Soochow University, Suzhou, Jiangsu Province 215123, China

[2]Department of Chemical Engineering and Biological Engineering, Monash University, Clayton, Victoria 3800, Australia

[3]Southeast University-Monash University Joint Research Institute, Suzhou Industrial Park, Suzhou, Jiangsu Province 215123, China

Correspondence
Jie Xiao, School of Chemical and Environmental Engineering, College of Chemistry, Chemical Engineering and Materials Science, Soochow University, Suzhou, Jiangsu Province 215123, China.
Email: jie.xiao@suda.edu.cn

Funding information
National Natural Science Foundation of China, Grant/Award Number: 21978184; Jiangsu Innovation and Entrepreneurship (Shuang Chuang) Program; Jiangsu Specially-Appointed Professors Program; Priority Academic Program Development (PAPD) of Jiangsu Higher Education Institutions

Abstract

Mathematical modeling of mass transfer and absorption in the small intestine has been a challenging task. Systematic review and analysis of existing efforts indicate the need to pursue a reliable predictive model that is physically sound and computationally efficient. With the consideration of 3D intestinal inner wall structure, this work rigorously derives an absorption model that can be used as a source term in a 1D distributed model, conventionally called the diffusion–convection–reaction model. Moreover, computational fluid dynamics simulations are carried out to generate *in silico* experimental data for quantification of the mass-transfer coefficient in the absorption model. This model facilitates a better understanding of the intricate influence of intestinal morphology and motility on mass transfer and absorption in the intestine. Rat duodenum featuring a villous structure and pendular movement is selected as an example to demonstrate the capability of this approach.

KEYWORDS
diffusion–convection–reaction (DCR) model, intestine, mass transfer and absorption, motility, villi

1 | INTRODUCTION

Intestinal absorption determines the bioavailability of nutrients and drugs. Understanding this important process can help identify the pathogeny of some food-related diseases, for example, Type 2 diabetes, obesity, and hyperlipidemia. Reliable quantification of absorption rate is crucial for the prediction of nutrient and drug concentrations in the blood, which are essential factors to be considered during food and drug development.

It has always been a challenging task to quantitatively investigate the absorption process. Over the past decades, various methodologies have been proposed to determine the intestinal permeability (m/s), a coefficient reflecting the rate of substance passing across the intestinal membrane.[1] *In vivo* experiments have been carried out, though limited by ethical reasons. Intestinal perfusion technique, including *in vivo* human intestinal perfusion[2] and *in situ* animal intestinal perfusion,[3] is a representative approach capable of quantifying the intestinal permeability. However, it has some intrinsic problems such as imposing an unrealistically high flow rate and being incapable of differentiating between consumptions by absorption and intestinal metabolism.[4] Moreover, it is impossible for *in vivo* experiments, human experiments, in particular, to identify the isolated effects of some characteristic features, such as intestinal morphology and motility.

Aiming to overcome these restrictions, many *in vitro* digestion systems have been developed as an alternative in recent years.[5–7] Most of these systems, however, simulate the processes in the intestinal lumen prior to absorption, for example, mixing, gastric emptying, hydrolysis, and so forth, and cannot take care of the complicated absorption mechanisms. A limited number of *in vitro* researches can

be identified to mimic the absorption process by using a semipermeable membrane that allows the passage of digested products (i.e., small molecules) and blocks undigested substrates.[8–10] For *in vitro* systems, it is difficult to implement complex geometrical features of a real small intestine, such as circular folds and villi, which affect the flow pattern and thus the mass transfer.[11,12] Even if some research groups used excised animal intestinal tissues[13] or cultured epithelial cell monolayer,[14] various movements of the intestinal walls, for example, segmentation and peristalsis, can hardly be implemented in those experiments.

In addition to the experimental study, lots of efforts have been devoted to mathematical modeling of the transport and evolution of food and drugs in the digestive tract.[6] Compared with *in vivo* and *in vitro* trials, *in silico* studies without ethical limitations can vastly reduce the cost and allow us to explore the influence of specific physiological structures or dietary properties on digestion. Comprehensive simulation results that are difficult to obtain through experiments can help us understand the underlying digestion and absorption mechanisms.

Computational fluid dynamics (CFD) models have been developed to explore a single or several physical and chemical phenomena in the intestinal lumen. They can reproduce various characteristic features of the intestinal tract *in silico* at different scales, such as axial propagating peristalsis,[15–18] circular nonpropagating contractions,[11,19,20] and curved tubular structure[17,18] at macroscale or villi movements[12,21–24] at microscale. The absorption was usually modeled as outward mass flux from the intestinal wall. These numerical studies revealed that the physiological features do have significant influences on mass transport and hence nutrient absorption. For example, a multi-physics model was developed by Zhang et al.[12] to investigate the impact of pendular movement on mass transfer and absorption in a rat intestine with villi on its inner wall. Since solving partial differential equations (PDEs) is computationally expensive, which is especially true for 3D cases with complicated geometry, it is impossible to use CFD models for instantaneous prediction of the absorption rate of nutrients or drugs. Note that for some applications, real-time prediction is mandatory. For instance, the feedback control of insulin injection for Type 1 diabetics is based on the real-time prediction of glucose absorption and the resulting blood glucose level.[25]

Without capturing the complicated fluid flow, the other set of approaches are lumped or distributed parameter models, which are ordinary differential equations (ODEs) or one-dimensional partial differential equations (1D PDEs), respectively. By sacrificing detailed spatial distribution information, they are computationally efficient and allow us to investigate the phenomena in a much larger system, for example, blood sugar regulation of the human body. Hence, they have wide application in the fields of pathology, pharmacology, and nutrition science, and so on. In these models, absorption is modeled as a sink term in the mass conservation equation, for example, the 1D diffusion–convection–reaction (DCR) model. To the extent of our knowledge, the derivation of the formula for the sink term (i.e., the absorption model) together with its associated parameters in a 1D model can hardly be identified. There are many questions that need to be answered or clarified. How to convert absorption flux on the intestinal wall in the 3D space to absorption rate in a 1D model? How to take into account intestinal morphology such as villi in the absorption model? How to determine key parameter values in the absorption model? What are the correlations between physiological features (e.g., morphology and motility) and absorption model parameters? Pursuing answers to these questions is critical for obtaining an in-depth understanding of the absorption process and rational use of the model for reliable prediction.

The focus of the current work is the characterization and investigation of *in vivo* chemical species' transport in the intestinal lumen followed by their absorption by the intestinal wall to enter the blood circulation. The chemical species modeled in this work are nutrients or drugs that can be directly absorbed by the intestine. Although multiple complex physical and chemical processes (e.g., breakdown of food or drug particles, and enzymatic reactions) may be involved to produce those chemical species, they are out of the scope of the current work. In the following text, the lumped and 1D distributed parameter models are first thoroughly reviewed. By organizing and analyzing these models, issues that need to be addressed are pointed out. After that, detailed derivations of our new absorption model are presented, which is followed by the approach for key parameter determination. Finally, the method is successfully applied to the study of absorption in rat duodenum. The influences of some physiological factors (such as villi length and motility) on absorption are investigated to reveal underlying mechanisms.

2 | REVIEW AND ANALYSIS OF REPORTED MODELS

Table 1 summarizes lumped and 1D distributed parameter models for mass conservation in the small intestine published in the open literature. The original key equations together with variable definitions are listed in columns 3 and 4. Based on the way to quantify the absorption behavior, these models are classified into five categories. For models in the same category, a general form of the equation is summarized in column 5 to capture their intrinsic connections.

Type 1 is the lumped parameter model that describes a digestive organ as a fully mixed tank reactor. These models usually follow a multi-compartmental simulation approach, which divides a system (i.e., the digestive tract) into several anatomical compartments (e.g., stomach, duodenum, jejunum, and ileum) and considers mass transport among them. The substance is assumed to be uniformly distributed throughout the compartment. The transport rate of a specific substance between two compartments generally depends on its amount in the source compartment. For this type of model, the intestinal absorption rate, Q, depends on the real-time amount of substances in the small intestine, M, which can be obtained by solving the ODEs of mass conservation. The absorption rate coefficient is usually assumed to be a constant, K, indicating a simple linear relationship between Q and M. Although these models can estimate the absorption rate, they all have a significant limitation, that is, the assumption

TABLE 1 Lumped and distributed parameter models for intestinal absorption.

	Ref. index	Model	Variable definition	Classification
I-1	26	Absorption rate (mmol/min): $U_G(t)=\frac{A_G}{t_{max,G}}\frac{D_G t e^{-t/t_{max,G}}}{t_{max,G}}$	A_G—carbohydrate bioavailability (−) D_G—amount of carbohydrates digested (mmol) $t_{max,G}$—time-of-maximum appearance rate of glucose in the accessible glucose compartment (min)	Lumped parameter model (fully mixed tank model without spatial distribution) $\frac{dM(t)}{dt}=-KM(t)+Q_{empt}(t)$ $Q(t)=KM(t)$
I-2	27	Change in mass in the gut (mg/min): $\dot{Q_{gut}}(t)=-k_{abs}Q_{gut}(t)+k_{empt}(Q_{sto})Q_{sto2}(t)$ Absorption rate (mg/min): $Ra=fk_{abs}Q_{gut}(t)$	k_{abs}—rate constant of intestinal absorption (s^{-1}) k_{empt}—rate of gastric emptying (s^{-1}) f—fraction of the intestinal absorption which actually appears in plasma (−)	
I-3	28	Change in mass in the duodenum and proximal jejunum (g/min): $\frac{dm_{prot3}}{dt}=\frac{\theta_{23}}{V_2}(m_{caswpd2}+m_{wpn2})-(k_{34}+k_{abs})m_{prot3}$ Change in mass in the distal jejunum: $\frac{dm_{prot4}}{dt}=k_{34}m_{prot3}-(k_4+k_{abs})m_{prot3}$	θ_{23}—gastric emptying flux (ml/min) V_2—volume of the second stomach compartment (ml) k_{34}—transit rate constant toward the distal jejunum (min^{-1}) k_4—transit rate constant toward the large intestine (min^{-1}) k_{abs}—rate constant of amino acid absorption (min^{-1})	
II-1	29	The fraction absorbed (−): $-\frac{dM}{dt}=2\pi RP_e\int_0^L C_b dz$ for a complete radial mixing model: $C_b=C_0e^{2A_n z/L}$ The absorption number is defined as: $A_n=\frac{L}{R}\frac{P_e}{\langle v_z\rangle}$	P_e—effective drug permeability (m/s), which is essentially mass-transfer coefficient $R\&L$—radius and length of the small intestine (m) $\langle v_z\rangle$—mean axial fluid velocity (m/s) C_b—bulk concentration (mg/m^3) C_0—inlet concentration (mg/m^3)	Distributed parameter model (concentration variation along axial direction) $C=f(z,t)$ $Q(t)=2\pi RP_e\int_0^L C dz$
III-1	30	$\frac{\partial C}{\partial t}=\alpha\frac{\partial^2 C}{\partial x^2}-\beta\frac{\partial C}{\partial x}-\gamma C$ $\alpha=D_e;\beta=\frac{Q}{\pi r^2};\gamma=\frac{2P_e}{r}$; Initial condition: $C(x,0)=0$ Four types of boundary conditions: $C(0,t)=C_0$ or C_0-kt or $C_0e^{-k_1 t}$ or C_0e^{-kt} $(k=\infty)$	D_e—effective diffusion coefficient (cm^2/s) P_e—apparent permeability (cm/s) Q—bulk fluid flow rate (cm^3/s) r—radius of the intestinal lumen (m)	Distributed parameter model (absorption mathematically modeled as volumetric reaction in the DCR model, concentration variation along axial direction, constant rate coefficient) $\frac{\partial C(z,t)}{\partial t}=D\frac{\partial^2 C(z,t)}{\partial z^2}-v\frac{\partial C(z,t)}{\partial z}-KC(z,t)$ $K=\frac{2\alpha}{R}k$ $Q(t)=\pi R^2 K\int_0^L C(z,t)dz$
III-2	31	$\frac{\partial \overline{C}(z,t)}{\partial t}+\overline{U}^*\frac{\partial \overline{C}(z,t)}{\partial z}=\overline{D}^*\frac{\partial^2 \overline{C}(z,t)}{\partial z^2}-\overline{K}^*\overline{C}(z,t)$ Initial condition: $\overline{C}(z,0)=\begin{cases}\overline{A}^*C_0, & 0\le z\le l_0\\ 0, & l_0\le z\le L\end{cases}$ Boundary condition: $\frac{\partial \overline{C}}{\partial z}\|_{z=0}=\frac{\partial \overline{C}}{\partial z}\|_{z=L}=0$ The total mass of drug in lumen (μg): $M(t)=\pi R_0^2\int_0^L \overline{C}(z,t)dz$ The mass of drug absorbed (μg): $M_A(t)=(1-E_H)e^{-k_c t}\overline{K}_A^*\int_0^t e^{k_c t}M(t)dt$	$\overline{U}^*$—mean axial velocity (m/s) $\overline{K}^*$—disappearance rate constant related to absorption and degradation (s^{-1}) $\overline{A}^*$—apparent or "fictitious" initial condition (−) E_H—hepatic extraction ratio due to first-pass metabolism in the liver (−) k_c—rate constant of therapeutic elimination from the body (s^{-1}) $\overline{K}_A^*$—the additive contribution to $\overline{K}^*$ owing to absorption (s^{-1})	

(Continues)

TABLE 1 (Continued)

	Ref. index	Model	Variable definition	Classification
III-3	32	$\frac{\partial G(z,t)}{\partial t} = -\overline{u}\frac{\partial G(z,t)}{\partial z} + \frac{V_{max}S(z,t)}{K_m+S(z,t)} - \frac{2f}{r_m}KG(z,t)$ The mass-transfer coefficient (m/s): $K = 1.62\left(\frac{\overline{u}D^2}{Ld}\right)^{1/3}$ &$D = \frac{K_B T}{6\pi\mu r_0}$	V_{max}—maximum reaction rate (mM/min) K_m—Michaelis constant (mM) f—surface area increase due to folds, villi & microvilli (–) L&d—length and diameter of the small intestine (m) μ—viscosity (mPa s)	
III-4	33	$\frac{\partial SI_N(z,t)}{\partial t} = \begin{cases} \gamma Stom_N(t) - \overline{u}\frac{\partial SI_N(z,t)}{\partial z} - K_a SI_N(z,t) & if\ z = l_0 \\ -\overline{u}\frac{\partial SI_N(z,t)}{\partial z} & otherwise \end{cases}$ $A(t) = \int_{z=0}^{L} K_a SI_N(z,t)dz$ $\gamma = \begin{cases} 0 & if\ A(t) > A_{max} \\ \gamma_0 & otherwise \end{cases}$	γ—gastric emptying rate constant (s^{-1}), influenced by intestinal absorption rate $A(t)$ via a feedback mechanism $\overline{u}$—mean axial velocity, (m/s) K_a—absorption constant of the nutrients (s^{-1}) A_{max}—maximum absorption rate (g/s)	
IV-1	34	$\frac{\partial q}{\partial t} + u\frac{\partial q}{\partial z} = \gamma q$ Boundary condition: $q(0,t) = \begin{cases} \eta(t)/u & 0 \le t \le \theta \\ 0 & t \ge \theta \end{cases}$ $Ra(t) = f\int_0^L \gamma(z)q(z,t)dz$	q—the amount of intraluminal glucose per unit length (mmol/m) $\eta(t)$—rate of glucose delivery to duodenum (mmol/min) θ—time required for gastric emptying (min) f—the fraction appears in the plasma (–)	Distributed parameter model (absorption mathematically modeled as volumetric reaction in the DCR model, concentration variation along axial direction, space-varying rate coefficient) $\frac{\partial C(z,t)}{\partial t} = D\frac{\partial^2 C(z,t)}{\partial z^2} - v\frac{\partial C(z,t)}{\partial z} - K(z)C(z,t)$
IV-2	35	$\frac{\partial C_1(x,t)}{\partial t} = \frac{1}{a(x)}\frac{\partial}{\partial x}\left(\begin{matrix} a(x)dif(x)\frac{\partial}{\partial x}C_1(x,t) \\ -C_1(x,t)a(x)vel(x) \end{matrix}\right)$ $-\frac{CL_{i2}(x)C_1(x,t)}{a(x)} + \frac{CL_{o2}(x)C_1(x,t)}{a(x)}$	a—cross-sectional area (m^2) dif—effective diffusion (m^2/s) vel—velocity (m/s) CL_{i2}—diffusional clearance from the lumen when radial diffusion is rate limiting (m^2/s) CL_{o2}—diffusional clearance from the apical membrane into the lumen (m^2/s)	
V-1	36	$\frac{\partial n}{\partial t} = -\frac{a}{A(x)}\frac{\partial n}{\partial x} - k(x,t)n$	a—nutrient flow rate (m^3/min) A—cross-sectional area (m^2) n—concentration of a substrate (mol/cm) k—rate constant (min^{-1})	Distributed parameter model (absorption mathematically modeled as volume reaction in the DCR model, concentration variation along axial direction, space- and time-varying rate coefficient) $\frac{\partial C(z,t)}{\partial t} = D\frac{\partial^2 C(z,t)}{\partial z^2} - v\frac{\partial C(z,t)}{\partial z} - K(z,t)C(z,t)$
V-2	37	$\frac{\partial q_i(z,t)}{\partial t} = -v\frac{\partial q_i(z,t)}{\partial z} - R_i(z,t,c)$ $R_{glu}(z,t) = f\theta(z,t)r(z,t)k_i(z,t)\left(c_{glu}(z,t) - c_b(z,t)\right)$ $Ra(t) = \int_0^L R_{glu}(z,t)dz$ Boundary condition: $q_i(0,t) = \frac{\gamma S_i(t) + Q_{is}C_{sec,i}}{v}$	R_i—absorption rate per unit length (kg/(m s)) γ—half-time of emptying (s) Q_{is}—flow rate of intestinal secretion (m^3/s) f—surface area increase due to folds, villi & microvilli (–) θ—filling angle of the fluid in the tubular intestine (–) r—internal radius (m) k_i—mass-transfer coefficient (m/s)	

TABLE 1 (Continued)

	Ref. index	Model	Variable definition	Classification
V-3	38	$\frac{\partial G_{si}(z,t)}{\partial t} = -v(t)\frac{\partial G_{si}(z,t)}{\partial z} + r_{H,fast}(S_{fast}(z,t)) + r_{H,slow}(S_{slow}(z,t)) - \left(\frac{2}{R_{si}}\right) r_{ab}(G_{si}(z,t))$ $r_{ab}(G_{si}(z,t)) = \frac{r_{ab,max} G_{si}(z,t)}{K_{ab} + G_{si}(z,t)}$	$r_{H,fast}$—fast digestion rate of starch (g/(cm^3 min)) $r_{H,slow}$—slow digestion rate of starch (g/(cm^3 min)) r_{ab}—glucose absorption rate (g/(cm^2 min)) R_{si}—radius of the small intestine (cm) $r_{ab,max}$—maximum rate of absorption (g/(cm^2 min)) K_{ab}—saturation constant for absorption (g/cm^3)	

of instantaneously thorough mixing of substances in a compartment, which is far from the realistic condition in a digestive organ, the small intestine in particular.

Type II model considers the spatial distribution of substances along the gut. Different from Type I models, the total absorption rate is calculated by integrating the localized mass flux over the intestinal inner surface, which is usually assumed to be a cylindrical tube with a constant radius. Since the nutrient is indeed absorbed through the inner wall of the intestine, this approach is physically sound. However, it is a challenging task to obtain the mass flux, which is the product of drug permeability and localized concentration in their work. In order to better capture mass distribution along the intestine, one needs to model mass conservation in the lumen with the consideration of fluid flow, nutrient diffusion, reaction and absorption, which inspires efforts summarized below.

Since the small intestine has a tubular structure, it can be modeled as a plug flow reactor (PFR), where chyme advances axially through the tube with reaction and absorption taking place simultaneously. In this regard, the 1D diffusion–convection–reaction (DCR) equation has been widely used for describing mass distribution in the intestinal lumen. As shown in column 5 of Table 1, mathematically, these models treat absorption as a volume reaction, whose rate per unit volume is calculated as a rate coefficient K (1/s) times local nutrient concentration C (mol/m^3). Integration of the rate per unit volume over the lumen volume yields the overall absorption rate Q (mol/s). Different ways were reported to quantify the rate coefficient, which is presented below. Type III models adopt a constant rate coefficient. In Type IV models, the rate coefficient is a function of location, that is, the distance from the pylorus. Type V models implement a rate coefficient with both spatial and temporal variations.

For models summarized in Table 1, the DCR model is the only one that can capture different physical and chemical phenomena taking place in the lumen, which has the potential for offering a new understanding of digestion and absorption. However, the current way of formulating the absorption-related sink term as a volumetric reaction without rigorous justification is difficult for readers to understand the underlying physics. As a result, it becomes very confusing to see different ways to quantify the rate coefficient (see different models from Type III to Type V in Table 1). It remains a mystery that how the complex geometry of the intestinal inner surface and the motility can quantitatively affect mass transfer and absorption.

3 | MODEL DEVELOPMENT

The intestine has been typically described as a circular PFR with a smooth inner wall. The real system is more complicated. On one hand, the inner surface of the intestinal wall is usually not smooth, having hierarchical structures at multiple scales, such as circular folds, villi and microvilli (see Figure 1A). Since nutrients are absorbed through villous epithelium, the multiscale structures significantly enlarge the absorption area. On the other hand, motility of the intestine includes peristalsis, segmentation, and pendular movement. These movements

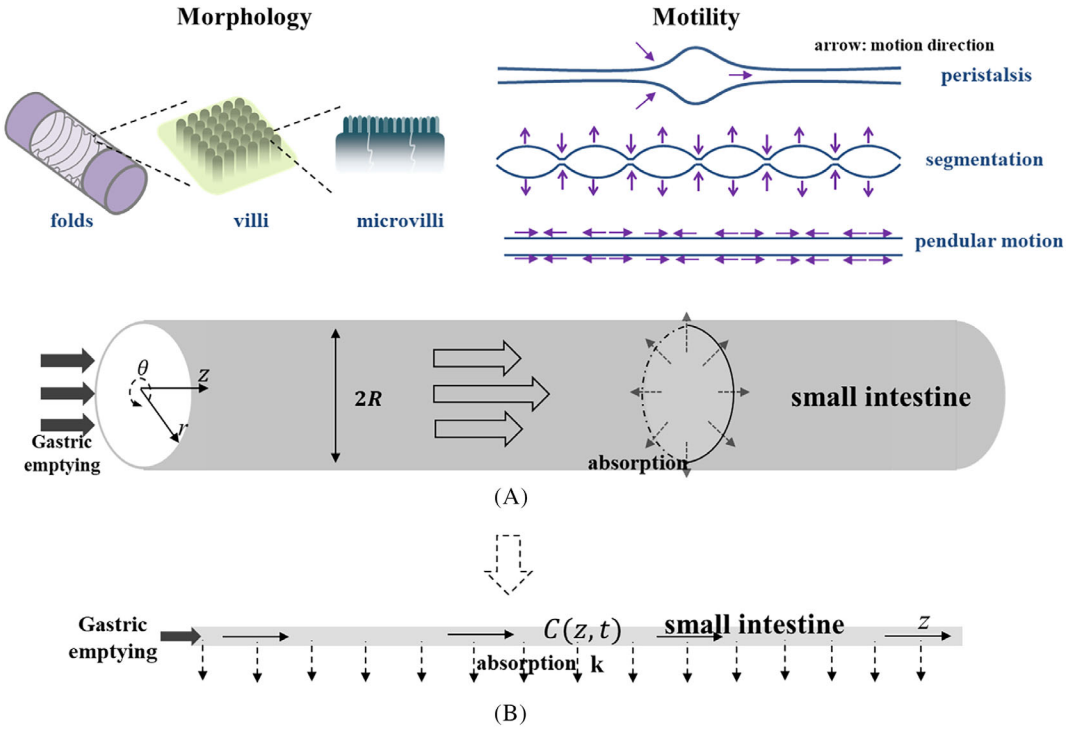

FIGURE 1 Model simplification from 3D to 1D: (A) 3D view of the small intestine with morphology and motility, and (B) 1D plot with consideration of the axial dimension only.

of the intestinal wall together with its hierarchical structure influence fluid flow and mass transfer in the lumen. In the following text, detailed derivations of a 1D distributed parameter DCR model for characterizing mass transfer and absorption in the intestine with consideration of the above-listed physiological features in 3D space are presented.

3.1 | Mathematical description of 1D distributed parameter model

For a 1D model shown in Figure 1B, it is assumed that the concentration is homogeneous in the radial and circumferential directions since the absorption of nutrients through the complete axisymmetric intestinal inner surface is predominantly determined by the concentration distribution along the axial direction. The mass conservation in the lumen of the small intestine can be described by the 1D DCR equation:

$$\frac{\partial C(z,t)}{\partial t} = D\frac{\partial^2 C(z,t)}{\partial z^2} - v\frac{\partial C(z,t)}{\partial z} - S(z,t) \tag{1}$$

The initial condition is:

$$C(z,0) = 0 \tag{2}$$

The boundary conditions at two ends are respectively:

$$C(0,t) = \frac{Q_{emp}(t)}{F}$$

$$\frac{\partial C}{\partial z}\Big|_{z=l} = 0 \tag{3}$$

Here $C(z,t)$ (mol/m^3) is the dynamic concentration of the nutrient along the intestine. $D\,(m^2/s)$ and v(m/s) are the diffusivity of the nutrient and the fluid flow velocity, respectively. $Q_{emp}(t)$ (mol/s) denotes the gastric emptying rate, that is, the flow rate of nutrient into the duodenum, whose value depends on dietary conditions in the stomach.[27,39] F (m^3/s) is the volume flow rate of liquid transported through the intestinal tract. In most previous models, $S(z,t)$ (mol/[m^3 s]) is the sink term corresponding to the consumption of nutrient due to reaction and/or absorption. In this work, the nutrient molecules that can be directly absorbed (e.g., glucose) are modeled, volumetric reaction is not considered. Our focus is the mathematical characterization of the sink term $S(z,t)$ due to absorption.

The absorption of nutrient into the blood is a multi-step process, that is, the transport of nutrient molecules in the lumen to the intestinal wall followed by their passage across the intestinal epithelium. The latter step is usually assumed to be instantaneous, and the rate-limiting step is the first one.[14,32] Therefore, the nutrient concentration on the intestinal inner surface is assumed to be zero and the absorption flux J (mol/[m^2 s]) can be expressed as:

$$J(z,t) = k(z,t)(C_b - 0) = k(z,t)C_b \tag{4}$$

where C_b (mol/m^3) represents the bulk concentration, which is equal to the inlet concentration; k(m/s) denotes the mass-transfer coefficient of the nutrient in the lumen and is affected by various factors, for example, fluid property, intestinal structure and motility, ambient flow, and so on.

As shown in Figure 1A, the total inner surface area of a cylindrical segment of length Δl is $\alpha 2\pi R\Delta l$, and thus the total absorption rate Q_a (mol/s) of this segment becomes:

$$Q_a(z,t) = \alpha 2\pi R\Delta l J(z,t) = \alpha 2\pi R\Delta l k(z,t) C_b \tag{5}$$

where R (m) is the radius of the small intestine and α (hereafter referred to as area-increase ratio) gives the ratio by which the absorptive area is increased due to intestinal inner surface structures, for example, the villi. To convert the absorption rate (in [mol/s]) to the volumetric consumption rate (in [mol/(m^3 s)]) that can be used as a sink term in Equation (1), Equation (5) should be divided by the cavity volume $\beta\pi R^2\Delta l$:

$$S(z,t) = \frac{2\alpha}{R\beta} k(z,t) C_b = K C_b \tag{6}$$

where β (hereafter referred to as volume-decrease ratio) denotes the ratio between the cavity volume of a rough tube (with consideration of inner surface structures) and that of a smooth tube. The consumption rate coefficient K (s^{-1}), which was used widely in previous studies (III-2,[31] III-3,[32] III-4,[33] IV-1,[34] V-1[36] in Table 1), is essentially:

$$K = \frac{2\alpha}{R\beta} k \tag{7}$$

The derivation steps above show how to convert the absorption rate on a 3D curved surface to the volumetric consumption rate used in a 1D DCR model. Equation (7) clarifies that the consumption rate coefficient depends not only on the mass-transfer coefficient k, but also on the geometrical features of the intestine, reflected by α, β, and R. It should also be pointed out that the change of intestinal inner surface structure influences not only α and β, but also k. Thus, the consumption rate will not simply be proportional to the absorption area in most cases. Furthermore, in addition to geometric features, motility of the intestine affects k as well, and other factors including ambient flow velocity and fluid properties also have an influence on the value of this parameter. The intricated correlations are given in Figure 2.

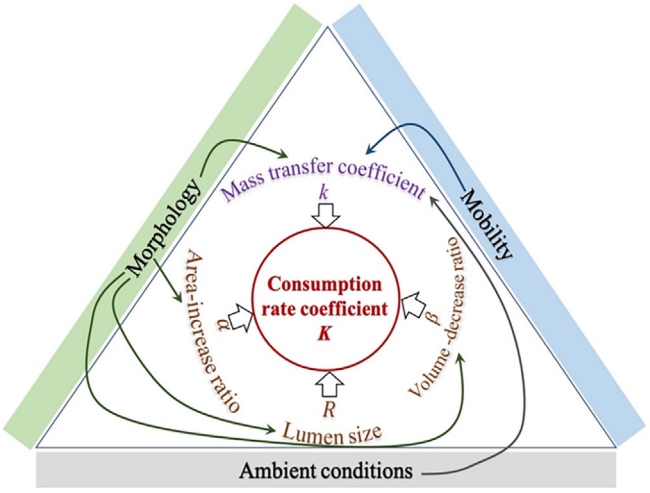

FIGURE 2 A schematic diagram showing the relationship between consumption rate coefficient and physiological properties.

3.2 | Quantification of absorption area and lumen volume

There are various structures, including circular folds, villi, and microvilli, on the inner surface of the small intestine. These structures offer greatly increased surface area for absorption. Meanwhile, they occupy a portion of the lumen volume.

The influences of intestinal surface morphology on absorption area and lumen volume can be quantified. Rat duodenum, which has no circular folds, is selected as an example. Villi are projections on the mucosa membrane that can enlarge the absorption area and reduce cavity volume. As shown in Figure 3, a healthy villus is a fingerlike structure, geometrically approximated by a hemisphere placed on the top of a cylinder. Without considering the area of its base, the surface area of a villus is:

$$\pi d_v\left(h_v - \frac{d_v}{2}\right) + \frac{\pi d_v^2}{2} = \pi d_v h_v \quad \text{if } h_v \geq \frac{d_v}{2} \tag{8}$$

where h_v(m) and d_v(m) are the length and the width of a villus, respectively. The height of a damaged villus may be less than the radius of its base. The geometry can then be approximated by a spherical cap of height h_v and base radius $\frac{d_v}{2}$. The surface area of such a damaged villus without considering its base becomes:

$$\pi\left(h_v^2 + \frac{d_v^2}{4}\right) \quad \text{if } 0 \leq h_v < \frac{d_v}{2} \tag{9}$$

Assuming that villi are uniformly distributed on the inner surface of the duodenum, the effective absorptive area of a segment of length Δl becomes

$$2\pi R\Delta l\omega_v \pi d_v h_v + 2\pi R\Delta l\left(1 - \frac{\pi d_v^2}{4}\omega_v\right) \quad \text{if } h_v \geq \frac{d_v}{2} \tag{10}$$

$$2\pi R\Delta l\omega_v \pi\left(h_v^2 + \frac{d_v^2}{4}\right) + 2\pi R\Delta l\left(1 - \frac{\pi d_v^2}{4}\omega_v\right) \quad \text{if } 0 \leq h_v < \frac{d_v}{2} \tag{11}$$

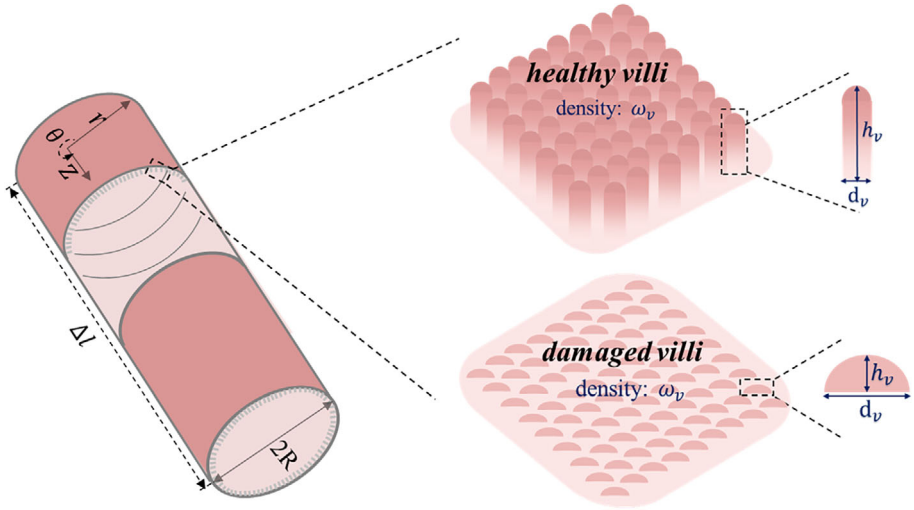

FIGURE 3 Multiscale structure of a rat duodenum segment modeled in this work.

where ω_v (m^{-2}) is the density of villi, that is, the number of villi per unit base area, and the latter terms in the two expressions above contain a deduction of the base area of villi. The area-increase ratio due to villi can be calculated as:

$$\alpha=\begin{cases}\dfrac{2\pi R\Delta l\omega_v\pi d_v h_v+2\pi R\Delta l\left(1-\dfrac{\pi d_v^2}{4}\omega_v\right)}{2\pi R\Delta l}=1+\pi\omega_v d_v\left(h_v-\dfrac{d_v}{4}\right) & \text{if } h_v\geq\dfrac{d_v}{2}\\ \dfrac{2\pi R\Delta l\omega_v\pi\left(h_v^2+\dfrac{d_v^2}{4}\right)+2\pi R\Delta l\left(1-\dfrac{\pi d_v^2}{4}\omega_v\right)}{2\pi R\Delta l}=1+\pi\omega_v h_v^2 & \text{if } 0\leq h_v<\dfrac{d_v}{2}\end{cases} \tag{12}$$

Similarly, the volume of a healthy villus is equal to the addition of the volume of a hemisphere and a cylinder:

$$\frac{\pi d_v^3}{12}+\frac{\pi d_v^2}{4}\left(h_v-\frac{d_v}{2}\right)=\frac{\pi d_v^2 h_v}{4}-\frac{\pi d_v^3}{24}\quad \text{if } h_v\geq\frac{d_v}{2} \tag{13}$$

A damaged villus geometrically approximated as a spherical cap has a volume of:

$$\frac{1}{6}\pi h_v\left(\frac{3}{4}d_v^2+h_v^2\right)\quad \text{if } 0\leq h_v<\frac{d_v}{2} \tag{14}$$

The total volume of villi in a segment of length Δl can be obtained by multiplying it by the number of villi:

$$\pi^2 R\Delta l\omega_v\left(\frac{1}{2}d_v^2h_v-\frac{1}{12}d_v^3\right)\quad \text{if } h_v\geq\frac{d_v}{2} \tag{15}$$

$$\pi^2 R\Delta l\omega_v\left(\frac{1}{4}d_v^2h_v+\frac{1}{3}h_v^3\right)\quad \text{if } 0\leq h_v<\frac{d_v}{2} \tag{16}$$

Then the volumetric ratio of the cavity of a rough intestinal tract to a smooth one can be quantified as:

$$\beta=\begin{cases}\dfrac{\pi R^2\Delta l-\pi^2 R\Delta l\omega_v\left(\dfrac{1}{2}d_v^2h_v-\dfrac{1}{12}d_v^3\right)}{\pi R^2\Delta l}=1-\dfrac{\pi\omega_v d_v^2}{2R}\left(h_v-\dfrac{d_v}{6}\right) & \text{if } h_v\geq\dfrac{d_v}{2}\\ \dfrac{\pi R^2\Delta l-\pi^2 R\Delta l\omega_v\left(\dfrac{1}{4}d_v^2h_v+\dfrac{1}{3}h_v^3\right)}{\pi R^2\Delta l}=1-\dfrac{\pi\omega_v h_v}{2R}\left(\dfrac{1}{2}d_v^2+\dfrac{2}{3}h_v^2\right) & \text{if } 0\leq h_v<\dfrac{d_v}{2}\end{cases} \tag{17}$$

3.3 | Quantification of mass transfer and consumption rate coefficients

The mass transfer behavior in the small intestine can be numerically investigated in detail by a CFD model. Herein a multi-physics model, which takes into account the villi in the rat duodenum, is taken as an example to show how to obtain the mass-transfer coefficient in the 1D DCR model. A detailed description of this model can be found in our previous publication.[12]

In this 2D axisymmetric system, the mass-transfer coefficient within the lumen can be obtained by rearranging Equation (4).

$$k=\frac{J}{C_b} \tag{18}$$

where J (mol/[m^2 s]) represents the flux of nutrient absorbed through the intestinal wall, that is, along the villi surface.

As reported in our previous studies,[12,24] the mass-transfer coefficient k varies along the villi surface and changes with time. Its average values can be derived for the sink term in the 1D DCR model. The spatial average over the rough boundary can be calculated as:

$$\bar{k}=\frac{\int_0^{\mathcal{L}}k d\delta}{\mathcal{L}} \tag{19}$$

Here δ is used to represent location, which gives distance along the rough boundary from the starting point of absorption.

TABLE 2 Parameter values for a rat duodenum used in this article.

Parameter		Value	References
Radius of the duodenum	R	3 mm	40
Flow velocity	v	0–2 × 10^{-4} m/s	41
Pendular activity frequency	f	0, 0.15–1.0 s^{-1}	42–44
Length of a villus	h_v	0–0.9 mm	45–49
Width of a villus	d_v	0.156 mm	50
Density of villi	ω_v	9 mm^{-2}	51

The temporal average of $\bar{k}$ over a period of motility is:

$$\bar{\bar{k}} = \frac{\int_0^T \bar{k} dt}{T} \tag{20}$$

where $\mathcal{L}$ (m) is the total length of the absorptive rough boundary and T (s) denotes the duration of a pendular activity.

Substituting the average mass-transfer coefficient into Equation (7) yields:

$$K = \frac{2\alpha}{R\beta}\bar{\bar{k}} \tag{21}$$

This method can help quantitively reveal the impacts of diverse physiological factors, such as villi length, motility, and ambient flow velocity, on mass transfer and absorption. Furthermore, to incorporate these influences explored by CFD simulation into the 1D DCR model, an empirical function of the mass-transfer coefficient depending on physiological parameters has also been derived in this work.

3.4 | Summary of differences between the new model and previous ones

Among the models reviewed in Table 1, models III-1,[30] III-2,[31] III-3,[32] III-4,[33] and V-2[37] are selected as control group models, since they essentially have a similar form of the absorption model (i.e., the sink term in the DCR equation), that is, the product of the mass-transfer coefficient k and concentration C multiplied by a coefficient ϕ.

$$S = \phi k C \tag{22}$$

where the coefficient ϕ is simply 1 (1/m) for models III-2 and III-4; model III-1 considers intestinal lumen radius R in ϕ (i.e., $\emptyset = \frac{2}{R}$); models III-3 and V-2 further take the increase of absorption area due to intestinal inner surface structure into account by using a constant ratio α, which gives $\emptyset = \frac{2\alpha}{R}$. Through rigorous derivation, ϕ in our new model becomes $\emptyset = \frac{2\alpha}{R\beta}$. The new model can capture quantitatively the influence of the intestinal microstructure on the increase of absorption area and the decrease of lumen volume, while the control group models either neglected this influence or adopted a constant area increase ratio. Furthermore, the new one can capture the relationship between the mass-transfer coefficient and key parameters that characterize representative physiological features of the intestine by using CFD simulations, *in silico* experimental design and data fitting methods, while control group models either conducted expensive experiments or adopted an empirical relationship for plug flow in a smooth tube that ignores the effect of villi on fluid flow and mass transfer. With these advantages, the new model will be more powerful in reliable prediction of intestinal absorption rate for a variety of living beings with specific physiological features, and will help save tremendous effort on expensive *in vivo* experiments.

4 | RESULTS AND DISCUSSION

The rat duodenum featuring pendular motility is selected to demonstrate the efficacy of the introduced methodology. The related physiological parameters are given in Table 2.

4.1 | Base case study

A base case with settings of villi length $h_v = 0.5$ mm, pendular frequency $f = 0.6\ s^{-1}$, and flow velocity $v = 1 \times 10^{-4}$ m/s has been selected to demonstrate the procedure to obtain the consumption rate coefficient K. According to Equations (12) and (17), the area-increase ratio α and volume-decrease ratio β can be calculated, respectively as 3.03 and 0.95.

By resorting to the 2D axisymmetric rat duodenum model, the absorptive flux J can be quantified. Figure 4A shows the spatial distributions of J along the rough surface of the intestine at two representative time instants (i.e., $T/2$ and T) during one cycle of the pendular movement. The nonuniform distribution of absorption flux indicates the nonuniform mass transfer behavior along the villi occupied intestinal surface (see insets in Figure 4A). According to Equation (18), mass-transfer coefficient k demonstrates the same distribution (see the right y-axis in Figure 4A). Maximum k can be identified at the top of the villi and the intervillous space has a k value close to zero. This observation implied that in this special case, nutrients can hardly reach the bottom of the villi.

The distribution of k evolves with time as well. Figure 4B shows the spatial average of k quantified by Equation (19) as a function of time. At $T/2$, maximum $\bar{k}$ can be identified. The temporal average in a pendular movement cycle $\bar{\bar{k}}$ can then be computed using Equation (20), which gives 2.61×10^{-7} m/s. Finally, Equation (21) offers the consumption rate coefficient K, that is, $5.76 \times 10^{-4}\ s^{-1}$.

4.2 | The influence of morphology

As one most important morphological parameter, the length of a villus was selected to explore its influence on mass transfer and absorption

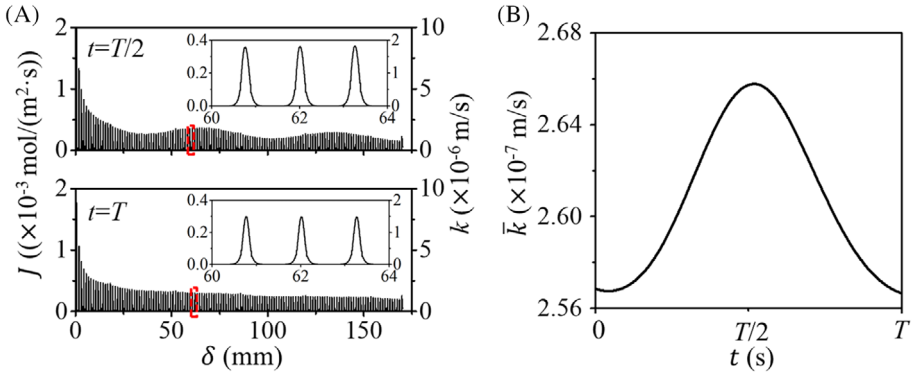

FIGURE 4 Distributions of absorptive flux and mass-transfer coefficient during one cycle of the pendular movement. (A) absorptive flux and mass-transfer coefficient distributions at $T/2$ and T, and (B) spatial average mass-transfer coefficient as a function of time. $T = 1.67$ s in this case.

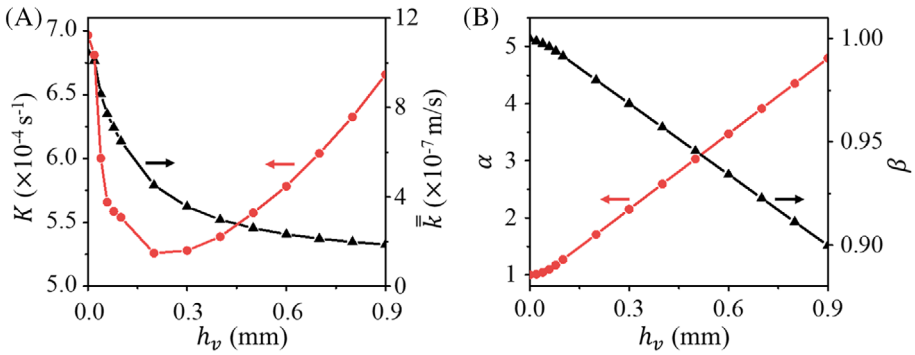

FIGURE 5 The influence of villi length on (A) the consumption rate coefficient and the average mass-transfer coefficient, and (B) the area-increase ratio and the volume-decrease ratio.

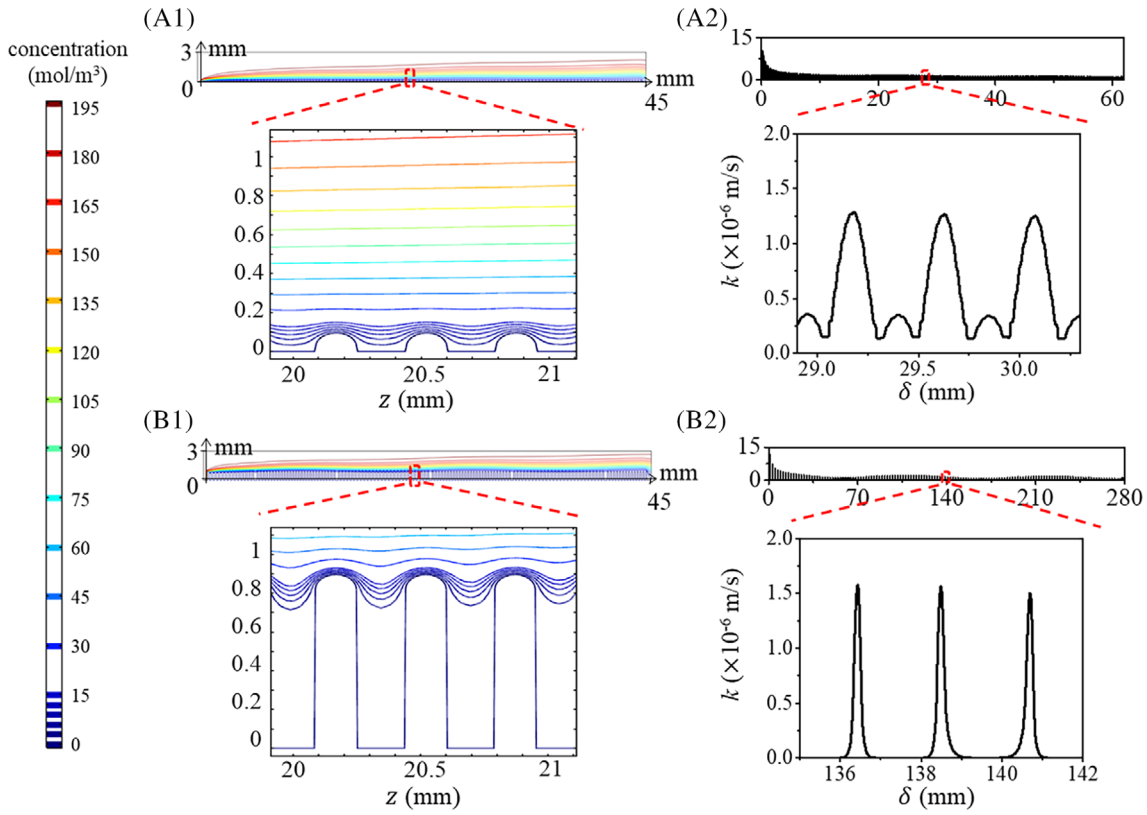

FIGURE 6 Concentration contours and mass-transfer coefficient distributions at $T/2$ when villi length is 0.1 mm (A) and 0.9 mm (B).

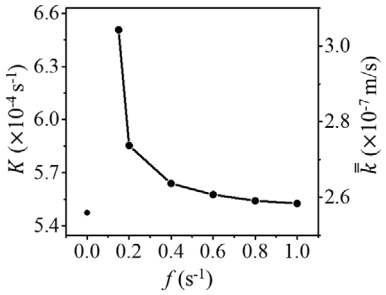

FIGURE 7 Influence of pendular frequency on the average mass-transfer coefficient and the consumption rate coefficient.

in the intestine. It was reported that the normal length of rat villi varies among individuals from 0.35 to 0.67 mm.[45–47] Some illnesses (e.g., sepsis, cholera, and noninfectious inflammation), however, can lead to shortened villi with deteriorated absorptive capacity[48] or extended villi with widened intercellular space.[49] Thus, the villi length explored in this work ranges from 0 to 0.9 mm.

It is interesting to find out that the consumption rate coefficient K is not a monotonic function of the villi length h_v, which indicates that increasing villi length may not always enhance nutrient absorption. As shown in Figure 5A, when the villi length is less than 0.2 mm, shorter villi offer a higher K value, that is, enhanced nutrient absorption. For the systems with villi greater than 0.2 mm, however, longer villi are preferred for better nutrient absorption.

According to Equations (12) and (17), both the area-increase ratio α and the volume-decrease ratio β are linear functions of the villi length when $h_v \geq d_v/2$. Figure 5B shows that increasing the length of villi leads to the increase of absorption area (and α) and the decrease of the cavity volume (and β). Evidently, the case of $h_v = 0$ corresponds to an intestine with a smooth inner surface, where both α and β are 1. Equation (21) tells us both the increase of α and the decrease of β contribute positively to the consumption rate enhancement (i.e., the increase of K).

As indicated earlier in Figure 2, in addition to the geometrical influences on K (reflected by α and β), varying villi length will also influence the mass transfer behavior (reflected by the average mass-transfer coefficient $\bar{\bar{k}}$). Evidenced by the data in Figure 5A, $\bar{\bar{k}}$ changes with h_v. It seems counter-intuitive that longer villi inhibit mass transfer in the intestine (see the decreasing $\bar{\bar{k}}$ with the increase of villi length in Figure 5A). To understand this phenomenon, the nutrient concentration distribution in the lumen and the mass-transfer coefficient distribution along the intestinal rough surface at $T/2$ for the cases with 0.1 and 0.9 mm villi are respectively plotted in Figure 6A,B. Longer villi can indeed lead to higher peak values of the mass-transfer coefficient (see the greater nutrient concentration gradient and higher k values close to the top part of 0.9 mm villi in Figure 6). It implies that the pendular movement of longer villi exerts a greater impact on the surrounding flow field and enhances mixing in the central region of the lumen, promoting the absorption at the top of villi. However, intervillous spaces increase with the increase of villi length (see the comparison between Figure 6A1,B1). Villi are closely distributed on the intestinal inner surface and stand at a right angle to the direction of bulk flow through the intestinal lumen. The mixing of the fluid in the intervillous space, particularly the bottom region, and hence the mass transfer could be quite limited.[52] The relatively stagnant intervillous space expands as the villous length increases. The enlarged plots in Figure 6A2,B2 show that although a 0.9 mm villus has a higher k value at its top part, k drastically decreases to around 0 along the villous body surface and remains to be negligible in the intervillous region. It is not the case for the system with 0.1 mm villi, where nutrients can be transferred to the intervillous region and be absorbed by the intestinal surface between two adjacent villi (see the nonzero k between two villi in Figure 6A2). As a result, longer villi lead to smaller $\bar{\bar{k}}$ (Figure 5A). This comparison also tells us that although the intestine with longer villi offers a larger total surface area, the effective surface for absorption, however, is actually smaller as compared with the shorter villi system due to the limitation on mass transfer in the intervillous space.

Now the mechanisms for the nonmonotonic relationship between K and h_v can be explained. K is influenced by both the geometric factor (α and β) and the mass transfer behavior ($\bar{\bar{k}}$) (see Equation 21). Increasing villi length leads to the increase of α/β, but the decrease of $\bar{\bar{k}}$. When the villi length is less than 0.2 mm, the influence of mass transfer on K is dominant. But when villi are longer than 0.2 mm, the geometric influence on K (caused by varying villi length) becomes dominant instead.

4.3 | The influence of motility

The pendular movement is selected to explore motility influence on mass transfer and absorption. The frequency of longitudinal contractions normally occurred along the rat duodenum has been measured to be 0.56–0.64 s^{-1} by the spatiotemporal mapping technology.[42] However, the longitudinal movement in the rat intestine is likely to be affected by various factors, for example, acceleration by atropine[43] and inhibition by tetrodotoxin.[44] The frequency of pendular movement investigated in this work ranges from 0.15 to 0.9 s^{-1}.

As the size of villi does not change in this set of experiments (i.e., 0.5 mm), the constant values of α and β are respectively 3.03 and 0.95. Figure 7 shows the average mass-transfer coefficient and consumption rate coefficient against pendular frequency. Since the ratio of these two coefficients remains unchanged, the two curves overlap with each other (see Equation 21).

As shown in Figure 7, when the frequency is 0 (i.e., without villi movement), the mass-transfer coefficient is lower than the cases with villi movements. It suggests that the villi movement promotes mass transfer, which is understandable because the movement of villi enhances mixing of fluids adjacent to the intestinal inner wall. When the frequency is higher than 0.15 s^{-1}, a higher frequency of movement leads to deteriorated mass transfer and hence lower absorption rate. This finding seems counter-intuitive as well. Pendular movement is a periodic lengthening and shortening of intestinal muscles in the axial direction. A detailed description and characterization method for

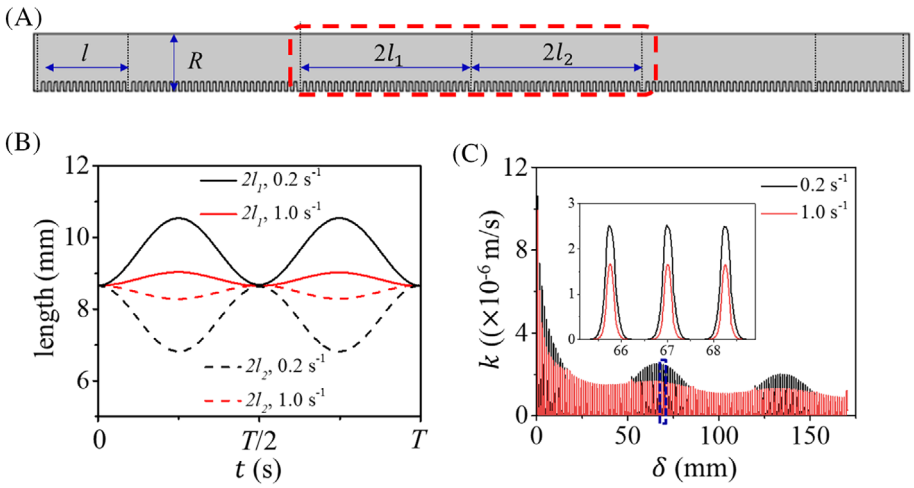

FIGURE 8 Comparison of two cases at pendular frequencies of 0.2 s^{-1} and 1.0 s^{-1}: (A) cross-sectional view of the rat duodenum, (B) evolution of the length of two adjacent sections that experience lengthening and shortening, respectively in one cycle, and (C) distribution of mass-transfer coefficient at $T/2$.

the movement can be found in our previous publication.[12] The velocity of the longitudinal movement of a villus at one position x is defined by a sinusoidal function:

$$v_v(x,t)=\frac{2l}{\pi}A_m sin\left(\frac{\pi}{2l}x\right)sin(2\pi ft) \tag{23}$$

where l(m) is the initial length of a section of the intestine (at a relaxed state in Figure 8A). This equation tells us that pendular frequency f does not affect velocity magnitude. Moving of villi at a higher frequency does not mean moving of villi at a higher velocity. Instead, a system of higher f offers less time in one cycle for the muscle to contract or expand, leading respectively to less intense shrinkage or enlargement of the intervillous space (Figure 8B). The mass transfer becomes less intense for the system at a higher frequency (Figure 8C).

4.4 | Empirical relationship for mass-transfer coefficient

As shown in Figure 2, mass-transfer coefficient is influenced by morphology, mobility, and ambient conditions. The previous two sections show how we can use CFD simulation to quantify the impact of villi length h_v and pendular frequency f on the mass-transfer coefficient $\bar{\bar{k}}$. CFD simulations are time-consuming, which motivates us to obtain an empirical relationship between $\bar{\bar{k}}$ and important independent variables (i.e., h_v, f, and ambient flow velocity v). A total number of 184 *in silico* experiments were designed, which include 180 ($6\times6\times5$) ones with experimental conditions respectively taken from the design spaces $h_v\in[0, 0.1, 0.3, 0.5, 0.7, 0.9]$ mm, $f\in[0.15, 0.2, 0.4, 0.6, 0.8, 1.0]$ s^{-1}, and $v\in[0, 0.5, 1, 1.5, 2]\times10^{-4}$ m/s. Four additional cases were also added to take care of short damaged villi with settings of $[h_v, f, v]=[d_v/8,\ 0.6\,s^{-1},\ 1\times10^{-4}\,m/s]$, $[2d_v/8,\ 0.6\,s^{-1},\ 1\times10^{-4}\,m/s]$, $[3d_v/8,\ 0.6\,s^{-1}, 1\times10^{-4}\,m/s]$, and $[4d_v/8, 0.6\,s^{-1}, 1\times10^{-4}\,m/s]$. All 184 simulation results have been plotted as experimental data points in Figure 9.

Four regression models were proposed to fit the 184 data points:

$$\text{Model R1}: \bar{\bar{k}}=\theta_1\exp(-\theta_2h_v-\theta_3f+\theta_4v)+\theta_5 \tag{24}$$

$$\text{Model R2}: \bar{\bar{k}}=\theta_1(h_v+\theta_2)^{-\theta_3}\exp(-\theta_4f)(v+\theta_5)^{\theta_6} \tag{25}$$

$$\text{Model R3}: \bar{\bar{k}}=\theta_1(h_v+\theta_2)^{-\theta_3}f^{-\theta_4}(v+\theta_5)^{\theta_6} \tag{26}$$

$$\text{Model R4}: \bar{\bar{k}}=\theta_1(h_v+\theta_2)^{-\theta_3}(f+\theta_4)^{-\theta_5}(v+\theta_6)^{\theta_7} \tag{27}$$

The principle of least squares was utilized to estimate parameter values (i.e., θ_i), which means the summation of the squared deviations (between experimental data and regression model predictions) was minimized. The identified optimal parameter values for each model are listed below. For model R1, $\theta_1=3.73\times10^{-7}$, $\theta_2=2628$, $\theta_3=0.044$, $\theta_4=5919$, $\theta_5=5.16\times10^{-8}$; for model R2: $\theta_1=1.74\times10^{-8}$, $\theta_2=1.62\times10^{-4}$, $\theta_3=0.83$, $\theta_4=0.046$, $\theta_5=1.09\times10^{-8}$, $\theta_6=0.35$; for model R3: $\theta_1=1.17\times10^{-8}$, $\theta_2=1.83\times10^{-4}$, $\theta_3=0.89$, $\theta_4=0.021$, $\theta_5=1.37\times10^{-8}$, $\theta_6=0.36$; for model R4: $\theta_1=1.77\times10^{-8}$, $\theta_2=1.57\times10^{-4}$, $\theta_3=0.82$, $\theta_4=2.54\times10^{-7}$, $\theta_5=0.022$, $\theta_6=1.05\times10^{-8}$, $\theta_7=0.35$.

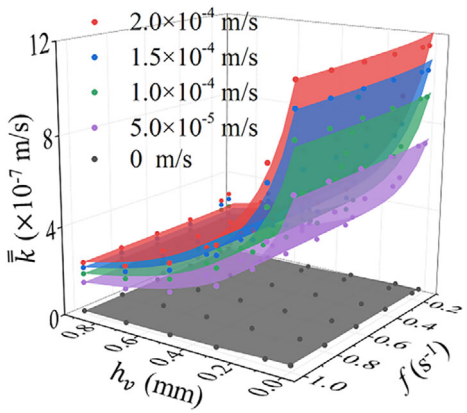

FIGURE 9 Evaluation of the proposed empirical function for the average mass-transfer coefficient. Dots are data from simulations. Surfaces are plotted using the derived empirical function.

After identification of optimal values for θ_i, error analyses were carried out to evaluate and compare the regression performance of these four models. In addition to mean absolute error (MAE) and root mean squared error (RMSE), two other metrics were also evaluated, that is, R-squared and adjusted R-squared. It was found that regression model R3 can offer the lowest values of MAE (3.82×10^{-8} m/s) and RMSE (3.94×10^{-8} m/s), and the highest values of R-squared (0.9917) and Adjusted R-squared (0.9914). The value of Adjusted R-squared can reach up to 0.9914, indicating a very satisfactory fitting performance. Thus, model R3 was finally selected as the empirical equation for $\bar{\bar{k}}$:

$$\bar{\bar{k}} = 1.17 \times 10^{-8}\left(h_v + 1.83 \times 10^{-4}\right)^{-0.89} f^{-0.021}\left(v + 1.37 \times 10^{-8}\right)^{0.36} \tag{28}$$

with h_v, f and v, respectively in m, s^{-1}, and m/s. Figure 9 shows model predictions as compared with the experimental data.

Figure 9 shows that higher ambient flow velocity promotes mass transfer (i.e., higher $\bar{\bar{k}}$), which is understandable. Equation (28) can then be used readily in the sink term (Equation 6) of the 1D DCR model to describe nutrient absorption in a rat duodenum featuring villi and pendular movement.

5 | CONCLUSION

Aiming at a physically-sound and computationally-efficient absorption model that can be used in a 1D DCR model, which governs mass conservation in the small intestine, this work critically reviewed existing efforts in this area and introduced a generic procedure for model derivation. By resorting to our derivation, the influence of 3D intestinal surface structure on absorption area and cavity volume can be rigorously quantified. The intricate correlations between the consumption rate coefficient and three determinant factors (i.e., morphology, motility, and ambient conditions) can be clarified.

This work sheds new light on our understanding of mass transfer and absorption in the small intestine. Rat duodenum which possesses a villous structure and pendular movement was selected as an example to demonstrate the power of this approach. It was found that villi length influences nutrient absorption by two mechanisms, that is, geometric impact and mass transfer impact. The geometric impact is dominant for cases with longer villi and the mass transfer impact becomes dominant for shorter villi systems. Results also show that a higher frequency of pendular movement leads to inhibited mass transfer and hence deteriorated nutrient absorption, which is mainly due to less intense volume change of intervillous space in such systems. Furthermore, an empirical correction between the consumption rate coefficient and three determinant factors has been obtained, which enables a fast prediction of absorption behavior in the rat duodenum. Nevertheless, all these findings have to be experimentally validated in the future when carrying out well-designed *ex vivo* or even *in vivo* intestinal absorption experiments becomes possible. The current *ex vivo* techniques[53–55] need to be improved to realize a better control of physiological features and a reliable measurement of spatially-distributed absorption data.

Note that the specific model (with the empirical relationship) derived here is just applicable to the rat duodenum featuring pendular movement. However, the idea and model derivation procedure are generic. In the future, following our approach, one can capture the influences of other physiological features (e.g., circular folds, segmentation movement, etc.). Beyond mass transfer phenomena, the chemical reactions during food digestion in the small intestine can also be taken into account in the future. Once coupled with an established glucose-insulin regulation model, the current model can be used to predict the blood glucose level. After experimental validation, it should be able to facilitate the development of functional foods and drugs for not only healthy adults but also specific groups of people with special physiological features and nutritional needs, such as infants, elderly, and patients with villous atrophy.

AUTHOR CONTRIBUTIONS

Yifan Qin: Data curation (supporting); formal analysis (supporting); investigation (supporting); writing – original draft (lead). **Xiao Dong Chen:** Conceptualization (supporting); supervision (supporting); writing – review and editing (supporting). **Aibing Yu:** Conceptualization (supporting); supervision (supporting); writing – review and editing (supporting). **Jie Xiao:** Conceptualization (lead); data curation (lead); formal analysis (lead); funding acquisition (lead); investigation (lead); methodology (lead); project administration (lead); supervision (lead); writing – review and editing (lead).

ACKNOWLEDGMENTS

We are grateful for the financial support from the National Natural Science Foundation of China (21978184), the "Jiangsu Innovation and Entrepreneurship (Shuang Chuang) Program," the "Jiangsu Specially-Appointed Professors Program," and the "Priority Academic Program Development (PAPD) of Jiangsu Higher Education Institutions." The authors thank Ms. Yanan Zhang for her preliminary effort on CFD model development. We also sincerely appreciate the constructive and in-depth comments with detailed suggestions from two anonymous reviewers.

DATA AVAILABILITY STATEMENT

The data that support the findings of this study are available from the corresponding author upon reasonable request.

ORCID

Xiao Dong Chen https://orcid.org/0000-0002-0150-0491
Aibing Yu https://orcid.org/0000-0002-5139-0657
Jie Xiao https://orcid.org/0000-0001-7842-7862

REFERENCES

1. Graziani C, Talocco C, Sire RD, et al. Intestinal permeability in physiological and pathological conditions: major determinants and assessment modalities. *Eur Rev Med Pharmacol Sci*. 2019;23:795-810.

2. Modigliani R, Bernier J. Absorption of glucose, sodium, and water by the human jejunum studied by intestinal perfusion with a proximal occluding balloon and at variable flow rates. *Gut*. 1971;12(3): 184-193.
3. Li H, Dong L, Liu Y, Wang G, Wang G, Qiao Y. Biopharmaceutics classification of puerarin and comparison of perfusion approaches in rats. *Int J Pharm*. 2014;466:133-138.
4. Qiu Y, Chen Y, Zhang GG, Yu L, Mantri RV. *Developing Solid Oral Dosage Forms: Pharmaceutical Theory and Practice*. 2nd ed. Elsevier Inc; 2016.
5. Dupont D, Alric M, Blanquet-Diot S, et al. Can dynamic in vitro digestion systems mimic the physiological reality? *Crit Rev Food Sci Nutr*. 2019;59(10):1546-1562.
6. Marze S. Bioavailability of nutrients and micronutrients: advances in modeling and in vitro approaches. *Annu Rev Food Sci Technol*. 2017;8: 35-55.
7. Wu P, Chen XD. On designing biomimic in vitro human and animal digestion track models: ideas, current and future devices. *Curr Opin Food Sci*. 2020;35:10-19.
8. Gonzalez C, Gonzalez D, Zuniga RN, Estay H, Troncoso E. Simulation of human small intestinal digestion of starch using an in vitro system based on a dialysis membrane process. *Foods*. 2020;9(7):913.
9. Karthikeyan J, Salvi D, Corradini MG, Ludescher RD, Karwe MV. Effect of bolus viscosity on carbohydrate digestion and glucose absorption processes: an in vitro study. *Phys Fluids*. 2019;31(11): 111905.
10. Tharakan A, Norton IT, Fryer PJ, Bakalis S. Mass transfer and nutrient absorption in a simulated model of small intestine. *J Food Sci*. 2010; 75(6):E339-E346.
11. Zha J, Zou S, Hao J, et al. The role of circular folds in mixing intensification in the small intestine: a numerical study. *Chem Eng Sci*. 2021; 229:116079.
12. Zhang Y, Wu P, Jeantet R, et al. How motility can enhance mass transfer and absorption in the duodenum: taking the structure of the villi into account. *Chem Eng Sci*. 2020;213:115406.
13. Priyadarshini SR, Arunkumar E, Moses JA, Anandharamakrishnan C. Predicting human glucose response curve using an engineered small intestine system in combination with mathematical modeling. *J Food Sci*. 2021;293:110395.
14. Lennernäs H, Palm K, Fagerholm U, Artursson P. Comparison between active and passive drug transport in human intestinal epithelial (Caco-2) cells in vitro and human jejunum in vivo. *Int J Pharm*. 1996;127(1):103-107.
15. Sinnott MD, Cleary PW, Arkwright JW, Dinning PG. Investigating the relationships between peristaltic contraction and fluid transport in the human colon using smoothed particle hydrodynamics. *Comput Biol Med*. 2012;42(4):492-503.
16. Sinnott MD, Cleary PW, Harrison SM. Peristaltic transport of a particulate suspension in the small intestine. *App Math Model*. 2017;44: 143-159.
17. Trusov PV, Zaitseva NV, Kamaltdinov MR. A multiphase flow in the antroduodenal portion of the gastrointestinal tract: a mathematical model. *Comput Math Methods Med*. 2016;2016:1-18.
18. Palmada N, Cater JE, Cheng LK, Suresh V. Experimental and computational studies of peristaltic flow in a duodenal model. *Fluids*. 2022; 7(1):40.
19. De Loubens C, Lentle RG, Love RJ, Hulls C, Janssen PW. Fluid mechanical consequences of pendular activity, segmentation and pyloric outflow in the proximal duodenum of the rat and the Guinea pig. *J R Soc Interface*. 2013;10(83):1-12.
20. Zhu T, Xia A, Lin K, et al. Numerical investigation of bio-inspired mixing enhancement for enzymatic hydrolysis. *Chem Eng Sci*. 2022;260: 117950.
21. Wang Y, Brasseur JG, Banco GG, Webb AG, Ailiani AC, Neuberger T. A multiscale lattice Boltzmann model of macro-to micro-scale transport, with applications to gut function. *Philos Trans Royal Soc A*. 2010;368:2863-2880.
22. Lentle RG, Janssen PWM, De Loubens C, Lim YF, Hulls C, Chambers P. Mucosal microfolds augment mixing at the wall of the distal ileum of the brushtail possum. *Neurogastroenterol Motil*. 2013; 25(11):881-e700.
23. Lim IYF. *Factors Influencing Mixing and Mass Transfer in the Small Intestine*. Doctor. Massey University; 2015.
24. Hua X, Zhang Y, Dong Z, Wang Y, Chen XD, Xiao J. Simulation and analysis of mass transfer and absorption process intensification by villi movement. *CIESC J*. 2020;71(5):2024-2034.
25. Kovatchev BP, Breton M, Dalla Man C, Cobelli C. In silico preclinical trials: a proof of concept in closed-loop control of type 1 diabetes. *J Diabetes Sci Technol*. 2009;3(1):44-55.
26. Hovorka R, Canonico V, Chassin LJ, et al. Nonlinear model predictive control of glucose concentration in subjects with type 1 diabetes. *Physiol Meas*. 2004;25(4):905-920.
27. Dalla Man C, Camilleri M, Cobelli C. A system model of oral glucose absorption: validation on gold standard data. *IEEE Trans Biomed Eng*. 2006;53(12):2472-2478.
28. Feunteun SL, Barbé F, Rémond D, et al. Impact of the dairy matrix structure on milk protein digestion kinetics: mechanistic modelling based on mini-pig in vivo data. *Food Bioproc Tech*. 2013;7(4):1099-1113.
29. Sinko PJ, Leesman GD, Amidon GL. Predicting fraction dose absorbed in humans using a macroscopic mass balance approach. *Pharm Res*. 1991;08(8):979-988.
30. Ni P, Ho N, Fox JL, Leuenberger H, Higuchi W. Theoretical model studies of intestinal drug absorption V. non-steady-state fluid flow and absorption. *Int J Pharm*. 1980;5(1):33-47.
31. Stoll BR, Batycky RP, Leipold HR, Milstein S, Edwards DA. A theory of molecular absorption from the small intestine. *Chem Eng Sci*. 2000; 55(3):473-489.
32. Moxon TE, Gouseti O, Bakalis S. In silico modelling of mass transfer & absorption in the human gut. *J Food Eng*. 2016;176:110-120.
33. Moxon TE, Nimmegeers P, Telen D, Fryer PJ, Impe JV, Bakalis S. Effect of chyme viscosity and nutrient feedback mechanism on gastric emptying. *Chem Eng Sci*. 2017;171:318-330.
34. Salinari S, Bertuzzi A, Mingrone G. Intestinal transit of a glucose bolus and incretin kinetics: a mathematical model with application to the oral glucose tolerance test. *Am J Physiol Endocrinol Metab*. 2011; 300(6):E955-E965.
35. Nagar S, Korzekwa RC, Korzekwa K. Continuous intestinal absorption model based on the convection-diffusion equation. *Mol Pharm*. 2017; 14(9):3069-3086.
36. Logan JD, Joern A, Wolesensky W. Location, time, and temperature dependence of digestion in simple animal tracts. *J Theor Biol*. 2002; 216(1):5-18.
37. Qin Y, Xiao J, Wang Y, Dong Z, Woo MW, Chen XD. Mechanistic exploration of glycemic lowering by soluble dietary fiber ingestion: predictive modeling and simulation. *Chem Eng Sci*. 2020;228: 115965.
38. Meraz M, Vernon-Carter EJ, Bello-Perez LA, Alvarez-Ramirez J. Mathematical modeling of gastrointestinal starch digestion-blood glucose-insulin interactions. *Biomed Signal Process Control*. 2022;77:103812.
39. Marciani L, Gowland PA, Spiller RC, et al. Gastric response to increased meal viscosity assessed by echo-planar magnetic resonance imaging in humans. *J Nutr*. 2000;130(1):122-127.
40. Lim YF, De Loubens C, Love RJ, Lentle RG, Janssen PW. Flow and mixing by small intestine villi. *Food Funct*. 2015;6(6):1787-1795.
41. Janssen PW, Lentle RG. Spatiotemporal mapping techniques for quantifying gut motility. In: Cheng LK, Pullan AJ, Farrugia G, eds. *New Advances in Gastrointestinal Motility Research*. Springer; 2013:219-241.
42. Lentle R, De Loubens C, Hulls C, Janssen P, Golding M, Chambers J. A comparison of the organization of longitudinal and circular

contractions during pendular and segmental activity in the duodenum of the rat and Guinea pig. *Neurogastroenterol Motil*. 2012;24(7):686-e298.
43. Gustafsson BI, Delbro DS. Neurogenic inhibition of duodenal and jejunal motility in the anaesthetized rat. *Eur J Pharmacol*. 1994;257(3):227-233.
44. Berčik P, Armstrong D, Fraser R, et al. Origins of motility patterns in isolated arterially perfused rat intestine. *Gastroenterology*. 1994;106(3):649-657.
45. Holm M, Powell T, Casselbrant A, Johansson B, Fändriks L. Dynamic involvement of the inducible type of nitric oxide synthase in acid-induced duodenal mucosal alkaline secretion in the rat. *Dig Dis Sci*. 2001;46(8):1765-1771.
46. Trevizan AR, Vicentino-Vieira SL, Paulo SW, et al. Kinetics of acute infection with toxoplasma gondii and histopathological changes in the duodenum of rats. *Exp Parasitol*. 2016;165:22-29.
47. Ilahi M, Khan J, Inayat Q, Abidi TS. Histological changes in parts of foregut of rat after indomethacin administration. *J Ayub Med Coll Abbottabad*. 2006;18(3):29-34.
48. Otani S, Coopersmith CM. Gut integrity in critical illness. *J Intensive Care*. 2019;7(1):1-7.
49. Mathan MM, Chandy G, Mathan VI. Ultrastructural changes in the upper small intestinal mucosa in patients with cholera. *Gastroenterology*. 1995;109(2):422-430.
50. Guseinov T, Guseinova S. Effect of dehydration on morphogenesis of the lymphatic network and immune structures in the small intestine. *Bull Exp Biol Med*. 2008;145(6):755-757.
51. Barry J, Ronald E. Mucosal surface areas and villous morphology of the small intestine of small mammals: functional interpretations. *J Mammal*. 1976;57(2):273-290.
52. Lentle RG, Janssen PW. *The Physical Processes of Digestion*. Springer Science & Business Media; 2011.
53. Ungell AL, Nylander S, Bergstrand S, Sjöberg Å, Lennernäs H. Membrane transport of drugs in different regions of the intestinal tract of the rat. *J Pharm Sci*. 1998;87(3):360-366.
54. Fagerholm U, Lindahl A, Lennernäs H. Regional intestinal permeability in rats of compounds with different physicochemical properties and transport mechanisms. *J Pharm Pharmacol*. 1997;49(7):687-690.
55. Hu Z, Wu P, Chen Y, Wang L, Jin X, Chen XD. Intestinal absorption of DHA microcapsules with different formulations based on *ex vivo* rat intestine and *in vitro* dialysis models. *Food Funct*. 2023;14:2008-2021.

How to cite this article: Qin Y, Chen XD, Yu A, Xiao J. New understanding from intestinal absorption model: How physiological features influence mass transfer and absorption. *AIChE J*. 2023;e18099. doi:10.1002/aic.18099